Spectroscopy of the low-lying states of the group III–V diatomics, AlP, GaP, InP, and GaAs via anion photodetachment spectroscopy

Harry Gómez, Travis R. Taylor,[a] Yuexing Zhao,[a] and Daniel M. Neumark[b]
Department of Chemistry, University of California and Chemical Sciences Division, Lawrence Berkeley National Laboratory, Berkeley, California 94720

(Received 17 July 2002; accepted 22 August 2002)

The low-lying electronic states of AlP, GaP, InP, and GaAs have been probed using anion photoelectron spectroscopy and zero electronic kinetic energy spectroscopy. We observe transitions from the anion $^2\Sigma^+$ and low-lying $^2\Pi$ states to the triplet ($^3\Sigma^-$ and $^3\Pi$ states) and singlet ($^1\Pi$, $^1\Sigma^+$, and $^1\Delta$ states) manifolds of the neutral species. The spectra of the triplet manifolds are particularly complex, with overlapping spin–orbit and vibrational progressions. Spin–orbit splittings, term energies, and vibrational frequencies are reported and compared to previous electronic structure calculations on the anions and neutrals, as well as to those parameters determined previously for the isovalent homonuclear diatomics Si_2, Ge_2, and Sn_2. © *2002 American Institute of Physics.* [DOI: 10.1063/1.1514050]

I. INTRODUCTION

The importance of III–V compounds in semiconductor devices has stimulated great interest in clusters of group III–V elements. While much of this work has focused on quantum confinement effects in very large clusters,[1,2] the electronic structure of the smallest molecular subunit, the diatomic, is not well characterized. In this paper we present systematic experimental studies that map out the low-lying electronic states of the XP^-/XP (X=Al,Ga,In) and $GaAs^-/GaAs$ diatomic systems, using anion photoelectron (PE) for all four species and zero electron kinetic energy (ZEKE) spectroscopy for $GaAs^-$.

Several experimental and theoretical studies of III–V diatomics have been reported. Boron nitride (BN) has received the most experimental attention of all the III–V diatomics. It has been shown to have a $^3\Pi$ ground state and the triplet states have been well studied by optical spectroscopy.[3–9] Photoelectron spectroscopy of BN^- yielded the relative energetics of the triplet and singlet manifolds of BN.[10] Photoelectron spectra of AlP^- and InP^- were reported but not analyzed by us as part of a study of larger Al_xP_y and In_xP_y clusters.[11,12] Lemire *et al.*[13] used resonant two-photon ionization spectroscopy to determine molecular constants for the spin–orbit components of the $3\,^3\Pi$ excited state of GaAs, while a laser-induced fluorescence study by Ebben and ter Meulen[14] showed AlN to have a $^3\Pi$ ground state. Li *et al.*[15,16] have studied several diatomic systems using matrix absorption experiments, finding vibrational fundamentals for GaX and InX (X=P,As,Sb), and determining the zero-field splitting of the $^3\Sigma^-$ ground states of InAs and InSb.[15] Jin *et al.* measured the first photoelectron spectrum of $GaAs^-$ from which they were able to extract an electron affinity of 2.1 ± 0.1 eV, but due to their low resolution they were unable to characterize the electronic structure of either the anion or neutral in much detail.

Much of the previous theoretical work on III–V diatomics has focused on GaAs,[17–21] but electronic structure calculations on AlP,[22,23] GaP[24,25] and InP[26] have also been reported. These studies considered bond lengths, vibrational frequencies, and energetics of the ground and low-lying electronic states in both the anionic and neutral species, and in some cases spin–orbit splittings were calculated. Figure 1 shows a qualitative picture of the anion and neutral electronic state energies for the four species considered here that emerges from these studies. The anion has a $^2\Sigma^+$ ground state and a low-lying $^2\Pi$ excited state. The neutrals are predicted to have a triplet manifold comprised of a $^3\Sigma^-$ ground state and $^3\Pi$ excited state, and a higher-lying singlet manifold comprised of the $^1\Pi$, $^1\Sigma^+$, and $^1\Delta$ states. The calculated splittings between states in a given manifold are quite small. For example, the calculated spacings between the $^3\Sigma^-$ and $^3\Pi$ states and the $^1\Pi$ and $^1\Sigma^+$ states for AlP are 0.11 and 0.13 eV, respectively, while the spacing between the singlet and the triplet manifold is calculated to be 0.43 eV.[22] This energy level diagram is similar to that previously determined for anionic and neutral Si_2, Ge_2, and Sn_2, the homonuclear isovalent species,[27–29] although some of the state orderings are predicted to be different in the homonuclear molecules.

Negative ion photodetachment offers a unique opportunity to map out the anion and neutral electronic states of the III–V diatomics, because the neutral triplet and singlet states can be accessed from the ground and low-lying anion states. The selection rules governing photoelectron spectroscopy are more relaxed than those for optical spectroscopy, with the major restriction being that only one-electron photodetachment transitions are observed, i.e., those neutral states that result from removal of a single electron from a negative ion molecular orbital with no additional rearrangement of the remaining electrons. As discussed in previous work on Si_2, Ge_2, and Sn_2, not all possible neutral←anion transitions in Fig. 1 are one-electron allowed, most notably the $^2\Sigma^+$

[a]Current address: Lam Research, 47131 Bayside Parkway, Fremont, CA 94538.
[b]Author to whom correspondence should be address. Electronic mail: dan@radon.cchem.berkeley.edu

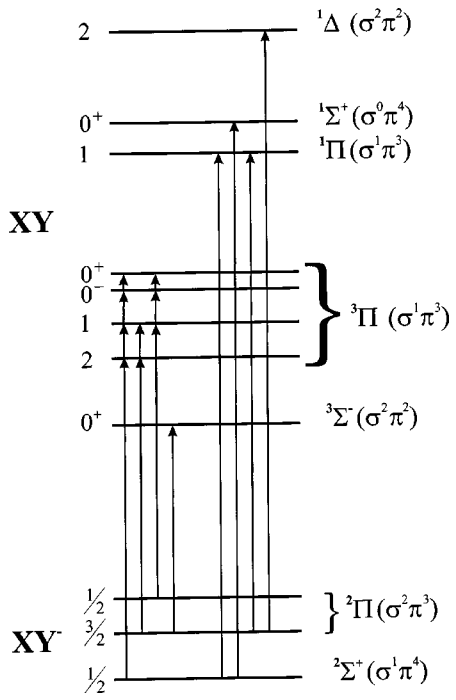

FIG. 1. Energy level diagram for XY^-/XY (X=Al, Ga, In and Y=P, As) as derived from *ab initio* calculations.

$\leftarrow{}^3\Sigma^-$ transition between the anion and neutral ground states.[27–31] Nonetheless, as shown in the work presented here, negative ion photodetachment can determine the energetics, vibrational frequencies, and spin–orbit splittings for nearly all of the states shown in Fig. 1. As a result, in addition to obtaining a complete picture of the low-lying electronic states for each species, one also can follow trends in the diatomic electronic structure with elemental composition, in particular the transition from Hund's case (a) to case (c) coupling as one moves down the group III and group V columns of the periodic table.

II. EXPERIMENT

The operation of the anion PE and ZEKE spectrometers is similar in principle. Both experiments generate negative ions with a laser ablation/pulsed-molecular beam source, mass-select them by time-of-flight (TOF), and photodetach them with a pulsed laser. However, the electron detection schemes are very different, providing much higher resolution (2–3 cm^{-1}) for ZEKE than in PE spectroscopy (PES) (65–80 cm^{-1}). Although the ZEKE technique has superior resolution one can only obtain photoelectron angular distributions from PES.

A. Photoelectron spectrometer

In the anion photoelectron spectrometer,[32,33] cluster anions are generated in a laser ablation/pulsed molecular beam source. For AlP clusters a rotating and translating pellet made of 50%–80% aluminum powder-200 mesh (Aldrich), 10%–30% red phosphorus (Aldrich), and 5%–20% KBr (Fisher Scientific) is ablated with the second harmonic (532 nm) of a pulsed Nd: yttrium–aluminum–garnet (YAG) laser. For the other clusters a rotating and translating single crystal disc of GaP, InP, or GaAs (Crystallode Inc.) is ablated with the second harmonic (532 nm) of a pulsed Nd: YAG laser. The laser pulses are typically 5.0–7.5 mJ/pulse before focusing onto the target with a 50 cm lens. The resulting plasma is entrained in a supersonic beam of helium and passes through a 1 3/4 in. long liquid nitrogen cooled clustering channel described elsewhere.[34] The gas pulse exits the clustering channel and passes through a skimmer into a differentially pumped region. Negative ions in the beam are extracted perpendicular to their flow direction by a pulsed electric field and injected into a linear reflection TOF mass spectrometer,[35,36] affording a mass resolution $m/\Delta m$ of 2000. Due to the natural isotope abundance of gallium (Ga^{69}:Ga^{71}, 100.0:66.4) each cluster stoichiometry has a mass distribution. In each case the most intense mass peak corresponding to $Ga^{69}As^{75}$ and $Ga^{69}P^{31}$ was studied.

Ions of the desired mass are selectively photodetached with photons having wavelengths of 355 nm (3.493 eV), 416 nm (2.977 eV), and 498 nm (2.490 eV). The 355 nm wavelength is obtained by tripling the fundamental of a pulsed Nd:YAG laser. The first and second Stokes lines generated by passing the third harmonic (355 nm) through a high pressure Raman cell filled with hydrogen (325 psig) produce the 416 and 498 nm light, respectively. The electron kinetic energy (eKE) distribution is determined by TOF analysis in a 1m field-free flight tube. The energy resolution is 8–10 meV at 0.65 eV eKE and degrades as $(\mathrm{eKE})^{3/2}$ at higher eKE. The data in electron kinetic energy is converted to electron binding energy (eBE) by subtracting it from the photon energy. All data are plotted in eBE as described by Eq. (1) where EA is the adiabatic electron affinity, E^0 is the internal energy of the neutral, and E^- is the internal energy of the anion.

$$\mathrm{eBE}=h\nu-\mathrm{eKE}=\mathrm{EA}+E^0-E^-. \tag{1}$$

The angular dependence of the photodetachment intensity for polarized light and randomly oriented molecules is given by Eq. (2)[37]

$$\frac{d\sigma}{d\Omega}=\frac{\sigma_{\mathrm{total}}}{4\pi}[1+\beta(\mathrm{eKE})\cdot P_2(\cos\theta)], \tag{2}$$

where θ is the angle between the electric vector of the photon and the direction of electron ejection, σ_{total} is the total photodetachment cross section and β(eKE) is the asymmetry parameter $(-1\leqslant\beta\leqslant 2)$. Each neutral←anion photodetachment transition has a characteristic asymmetry parameter that can sometimes be used to distinguish peaks of overlapping electronic transitions. The asymmetry parameter of a peak can be calculated[38] using Eq. (3)

$$l1;\text{-}2q\beta(\mathrm{eKE})=\frac{I_{0^\circ}-I_{90^\circ}}{\frac{1}{2}I_{0^\circ}+I_{90^\circ}}, \tag{3}$$

where I_{0° and I_{90° are the intensities of the peak taken at the polarization angles $\theta=0^\circ$ and 90°. The laser polarization can be rotated with respect to the direction of electron detection by using a half-wave plate.

B. ZEKE spectrometer

In the ZEKE spectrometer,[39,40] anions are generated in a similar manner to that described above, except the ablation/

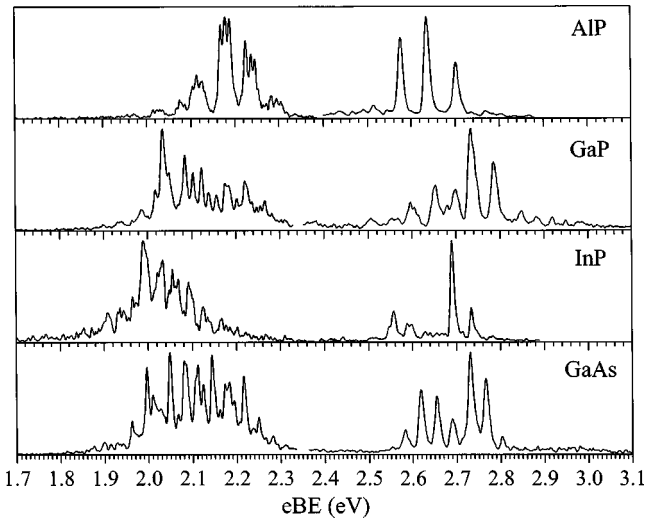

FIG. 2. Composite plots of the anion photoelectron spectra of XP (X=Al,Ga,In) and GaAs taken at the polarization angle of $\theta = \sim 54°$. See text for further description.

molecular beam source employs a rotating and translating rod instead of a disk. The anions pass through a 2 mm skimmer, are collinearly accelerated to 1 keV, and are then separated into clusters according to their masses in a 1 m TOF tube.

After they enter the detector region, the anion of interest is photodetached by an excimer-pumped dye laser. Once the photoelectrons are produced, a time delay between 200 and 350 ns is applied before they are extracted coaxially by a dc electric field of approximately 3 V/cm. During this time delay, electrons with velocity components perpendicular to the molecular beam drift out of the extraction zone. Hence, only electrons with trajectories parallel to the molecular beam or zero kinetic energy are extracted. The amount of energy they acquire during the extraction depends on their location in the extraction field, and thus their initial kinetic energies. A gated TOF detection scheme is used to selectively collect the near zero kinetic energy electrons. The resolution of this spectrometer in the absence of rotational broadening is 2–3 cm^{-1}.

The electron signal is normalized to laser power and ion signal, and averaged over 1200 laser shots per point. The dyes used to obtain the ZEKE spectrum of $GaAs^-$ were Coumarin 440, Coumarin 460, Coumarin 480, Coumarin 540, Rhodamine 590, and Rhodamine 610. The dye laser wavelength is calibrated by measuring the absorption spectra of an iodine cell or a Fe–neon cathode lamp.

III. RESULTS

Anion PE spectra of XP^-(X=Al,Ga,In) and $GaAs^-$ taken at a laser polarization angle of $\theta = \sim 57°$ [the ''magic angle,'' where $P_2(\cos\theta)=0$] are plotted in Fig. 2. Each spectrum is composed of two data sets, indicated by a break in the plot around ~2.4 eV. The data at lower eBE (left side) were taken at a wavelength of 498 nm for all the diatomics, while the data at higher eBE (right side) were collected at a wavelength of 416 nm for InP^- and 355 nm for the other diatomics. The two groups of peaks correspond to transitions to the triplet (left side) and singlet (right side) manifolds of neutral XP (X=Al,Ga,In) and GaAs as discussed in Sec. I and shown in Fig. 1.

Inspection of the PE spectra in Fig. 2 shows that the triplet manifolds for the XP^- series shift toward lower eBE as the size of X increases from Al to In, while the singlet manifolds remain around the same energy. In addition, the triplet manifolds for all four molecules are significantly more congested than the singlet manifolds. The singlet manifolds show two groups of peaks for all species except for AlP, where only three peaks are observed with similar spacing. The triplet manifolds show a fairly complex evolution as the atoms become heavier. In the AlP^- spectrum, several peaks are evidently partially resolved triplets; this pattern is not evident in the other PE spectra but more peaks appear in total, suggesting that the triplet components are more spread out and appear as individual peaks.

Figures 3 and 4 show expanded views of the triplet manifolds of XP (X=Al,Ga,In) and GaAs taken at polarization angles of $\theta = 0°$ (top) and $\theta = 90°$ (center), and a wavelength of 498 nm. The bottom panels show simulations which are discussed in Sec. IV. The $GaAs^-$ PE spectrum taken at $\theta = 90°$ is superimposed on the ZEKE spectrum. The peaks in the ZEKE spectrum are much narrower then in the PE spectra and every peak in the PE spectrum also appears in the ZEKE spectrum with similar intensity except for peaks A_1 and A'. Comparison of the $\theta = 0°$ and $\theta = 90°$ PE spectra and inspection of the anisotropy parameters β for each peak (top panel) shows a considerable variation in the photoelectron angular distribution among the peaks. Most notably, the single feature A, A_0, or A_1 dominates the $\theta = 0°$ PE spectra for all four species but is much less prominent, if visible at all, in the $\theta = 90°$ spectra. Moreover, anisotropy parameters for peaks at lower and higher eBE than peak A are different. Hence, it appears that the triplet manifolds are composed of three distinct neutral←anion electronic photodetachment transitions.

Figures 5 and 6 show expanded views of the singlet manifolds of XP (X=Al,Ga,In) and GaAs taken at polarization angles of $\theta = 0°$ (top) and $\theta = 90°$ (center), with simulations shown in the bottom panels. The photodetachment wavelength is 416 nm for InP and 355 nm for the other diatomics. The GaAs PE spectrum is superimposed on the ZEKE spectrum. Again, anisotropy parameters for each peak are shown in the top panel. There appear to be two distinct major progressions, labeled A and B, in each spectrum, with the peaks in progression B more intense at $\theta = 0°$ and the peaks in progression A more intense at $\theta = 90°$. Hence, at least two electronic photodetachment transitions contribution to each singlet manifold. The GaP spectrum shows two additional bands, C and D, at higher and lower eBE, respectively, than the two intense progressions. There is some evidence for additional, low intensity, high and low energy features in the spectra of the other diatomics, but no individual peaks can be resolved.

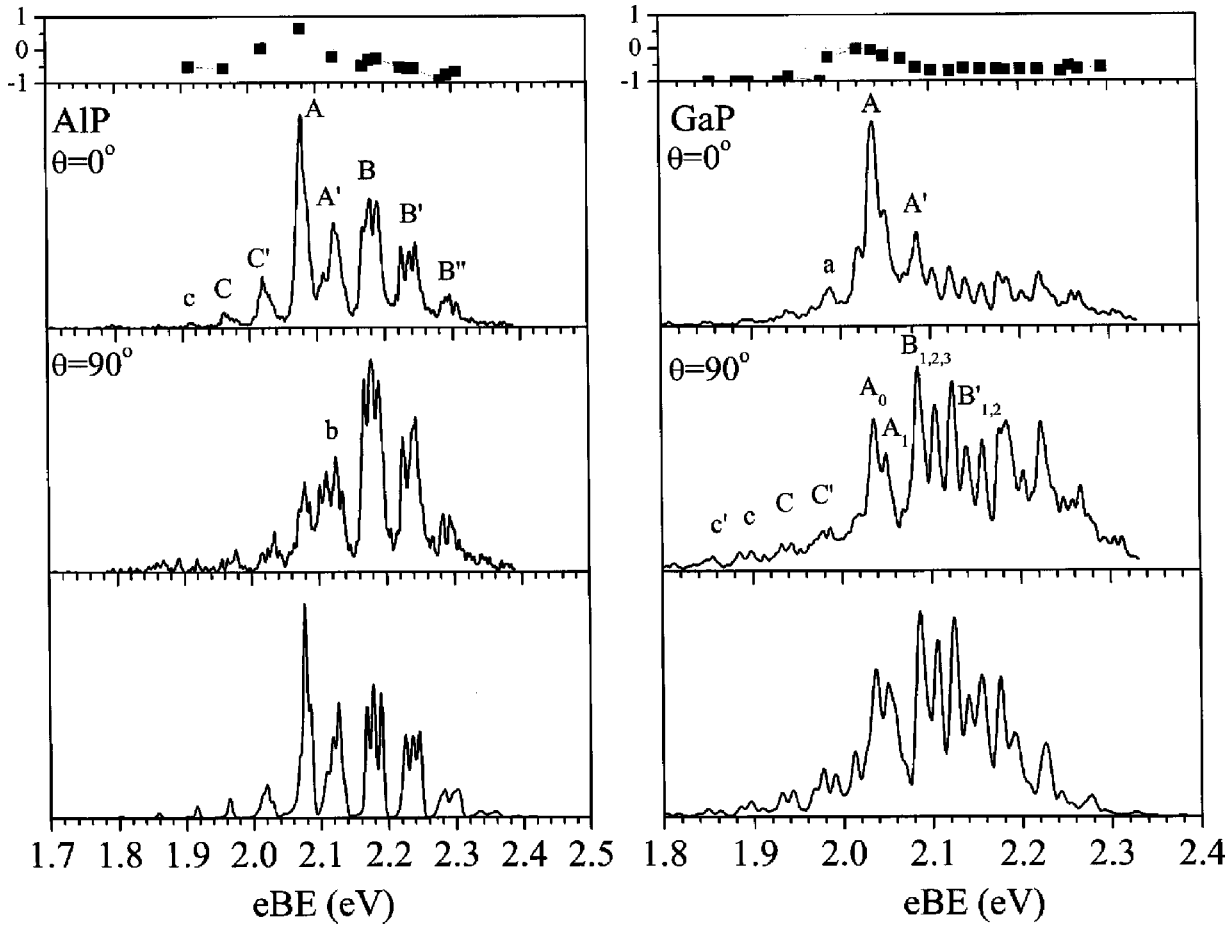

FIG. 3. Anion photoelectron spectra of AlP^- and GaP^- triplet manifold taken at 498 nm and laser polarization angles of $\theta=90°$ and $\theta=0°$. Experimental β parameters at the same photon energy are plotted in the top panel. FC simulations of the $\theta=0°$ spectrum of AlP and the 90° spectrum of GaP are shown in the bottom panel.

IV. ANALYSIS

A. General

Figure 1 is extremely useful for making a detailed assignment of the PE and ZEKE spectra. All of the III–V diatomics are calculated to have the same energy ordering of electronic states shown in Fig. 1,[17–20,22–25,41–44] except for InP where the $^1\Sigma$ and $^1\Delta$ states reverse their order.[26] For each energy level, the case (a) term symbol and highest molecular orbital occupancy is shown on the right, and the projection Ω of the total angular momentum on the internuclear axis is shown on the left. All one-electron allowed transitions from both low-lying anion states are shown in Fig. 1. Based on our previous work on the silicon and germanium dimers, we expect to observe a transition from Hund's case (a) to case (c) coupling as the atoms become heavier, leading, for example, to an observable splitting of the $^3\Pi_0$ state into its $^3\Pi_{0+}$ and $^3\Pi_{0-}$ components. Figure 1 shows the one-electron photodetachment transitions from the anion ground $^2\Sigma^+$ $(\ldots\sigma^1\pi^4)$ and low-lying $^2\Pi$ $(\ldots\sigma^2\pi^3)$ states. All neutral states are accessible from the anion ground state except those with the $(\ldots3\sigma^2 1\pi^2)$ electronic configuration; neutral states with this configuration include the ground $^3\Sigma^-$ and excited $^1\Delta$ states. From the anion $^2\Pi$ state, only the transition to the $^1\Sigma^+$ $(\ldots3\sigma^0 1\pi^4)$ state is forbidden by the one-electron selection rule.

More quantitative assignments and analyses were carried out by simulating vibrational and electronic structure seen in the PE and ZEKE spectra. Electronic term energies were varied to best match the experimental spectra. Within each electronic band, intensities of individual vibrational transitions are assumed proportional to their FC factors, $|\langle\nu'|\nu''\rangle|^2$, where $|\nu'\rangle$ and $|\nu''\rangle$ are neutral and anion harmonic oscillator wave functions, respectively. The vibrational frequencies are taken directly from the spectra, and the change in bond length upon photodetachment is varied to reproduce the length of the vibrational progression in the experimental spectrum. The anion vibrational temperature was also varied in order to reproduce hot bands in the spectrum originating from vibrationally excited anions. Typical vibrational temperatures used in this work range from 350 to 550 K. The resulting stick spectrum was then convoluted with a Gaussian function of width comparable to our experimental resolution, usually 8–15 meV.

We begin our analysis by considering the singlet manifolds for all four species. These are considerably easier to analyze than the triplet manifolds and provide information that facilitates analysis of the more complex triplet manifolds.

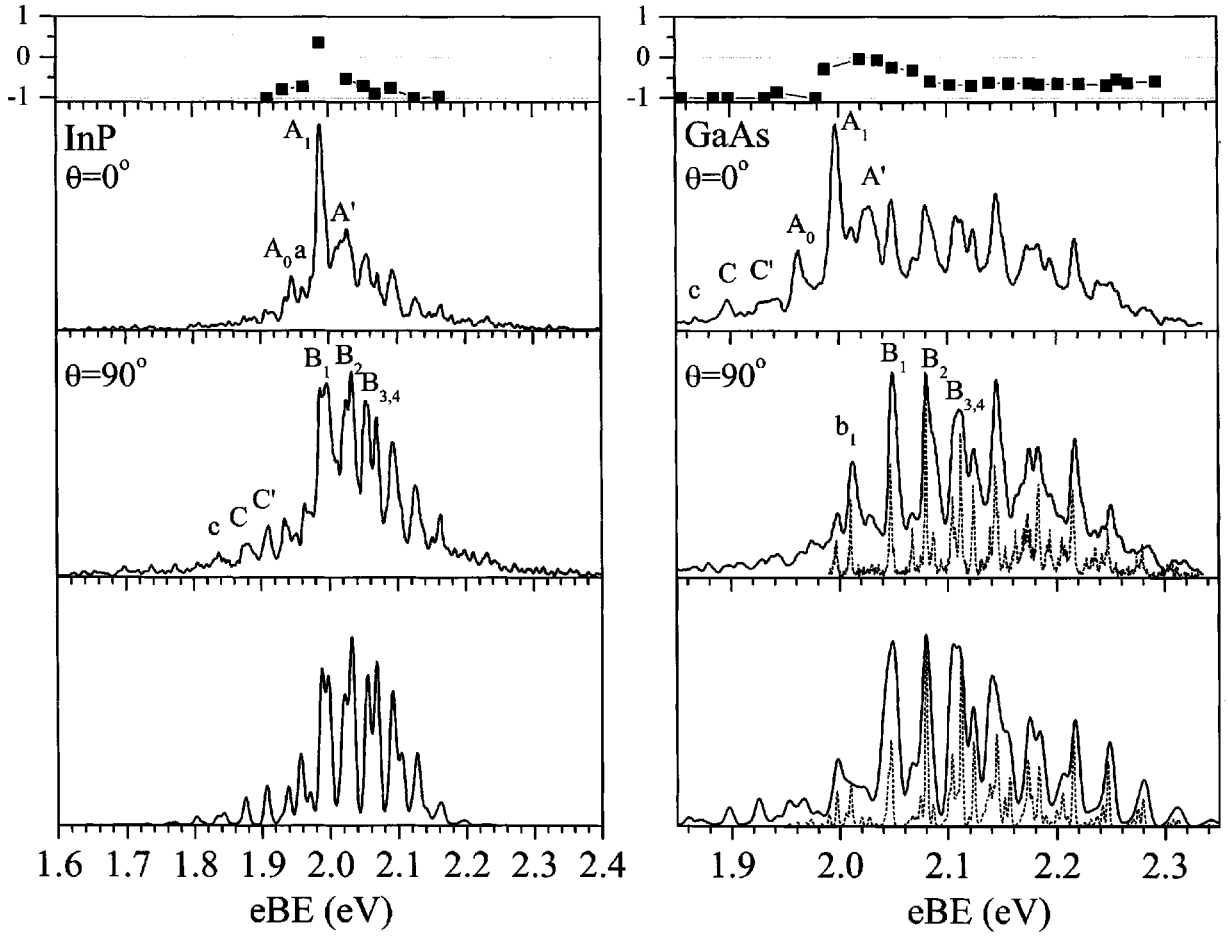

FIG. 4. Anion photoelectron spectra of InP^- and $GaAs^-$ triplet manifold taken at 498 nm and laser polarization angles of $\theta=90°$ and $\theta=0°$. Experimental β parameters at the same photon energy are plotted in the top panel. FC simulation of the $\theta=90°$ spectrum is shown in the bottom panel. Experimental and simulated ZEKE spectra of GaPs are shown as dotted lines and in the center and bottom panel.

B. Singlet manifolds

1. AlP

The anisotropy parameters for the AlP singlet manifold suggest that peaks *a* and *A* are from one electronic photodetachment band (''*A*''), and peaks *B*, *B′*, and *B″* are from another (''*B*''). Peaks *a* and *A* are separated by 516 cm^{-1}, peaks *A* and *B* are separated by 475 cm^{-1}, and peaks *B*, *B′*, and *B″* are separated by 540 cm^{-1}. The low intensity of peak *a* suggests it is a hot band electronic transition with origin at *A*, while the equal spacing of peaks *B*, *B′*, and *B″* suggests a vibrational progression with *B* as the origin.

With reference to Fig. 1, the neutral $^1\Pi$ and $^1\Sigma^+$ states are accessible via one-electron transitions from the anion $^2\Sigma^+$ state, whereas the neutral $^1\Pi$ and $^1\Delta$ states are accessible from the anion $^2\Pi$ state. The observation of only two strong bands in the singlet manifold of the AlP^- PE spectrum thus suggests that both originate from a single anion state.

Electronic structure calculations[22] on AlP^- predict a $^2\Sigma^+$ ground state with a vibrational frequency of 551 cm^{-1}, and a $^2\Pi$ excited state with a term value of 0.08 eV and a vibrational frequency of 465 cm^{-1}. The only calculation on the excited singlet states of AlP was done by Meier *et al.*[23] who found the $^1\Pi$, $^1\Sigma^+$, $^1\Delta$ states to have term energies of 0.46, 0.56, and 0.83 eV, and vibrational frequencies of 487, 528, and 374 cm^{-1}, respectively. The anion and neutral calculations are summarized in Table I. If both calculations are correct, then both bands originate from the anion $^2\Sigma^+$ state, since this state should be the most populated in the ion beam, and bands ''*A*'' and ''*B*'' would be assigned to the $^1\Pi \leftarrow {}^2\Sigma^+$ and $^1\Sigma^+ \leftarrow {}^2\Sigma^+$ photodetachment transitions, respectively. The observed vibrational spacing of band ''*B*,'' 540 cm^{-1}, is very close to the calculated frequency for the $^1\Sigma^+$ state, 528 cm^{-1}, consistent with this assignment. This assignment also yields a splitting of 0.058 eV between the neutral $^1\Pi$ and $^1\Sigma^+$ states, only slightly smaller than the calculated splitting of 0.10 eV.

If, on the other hand, both bands originated from the anion $^2\Pi$ state, then bands ''*A*'' and ''*B*'' would be transitions to the neutral $^1\Pi$ and $^1\Delta$ states, respectively. This alternate assignment is in more conflict with theory; the $^1\Pi - {}^1\Delta$ splitting would be much smaller than the calculated splitting of 0.37 eV, and the vibrational frequency of the $^1\Delta$ state (540 cm^{-1}) would be much larger than the calculated value of 374 cm^{-1}. For these reasons, the first assignment is preferred, indicating the anion has a $^2\Sigma^+$ ground state with vibrational frequency 516 cm^{-1} (the spacing between peaks *a* and *A*).

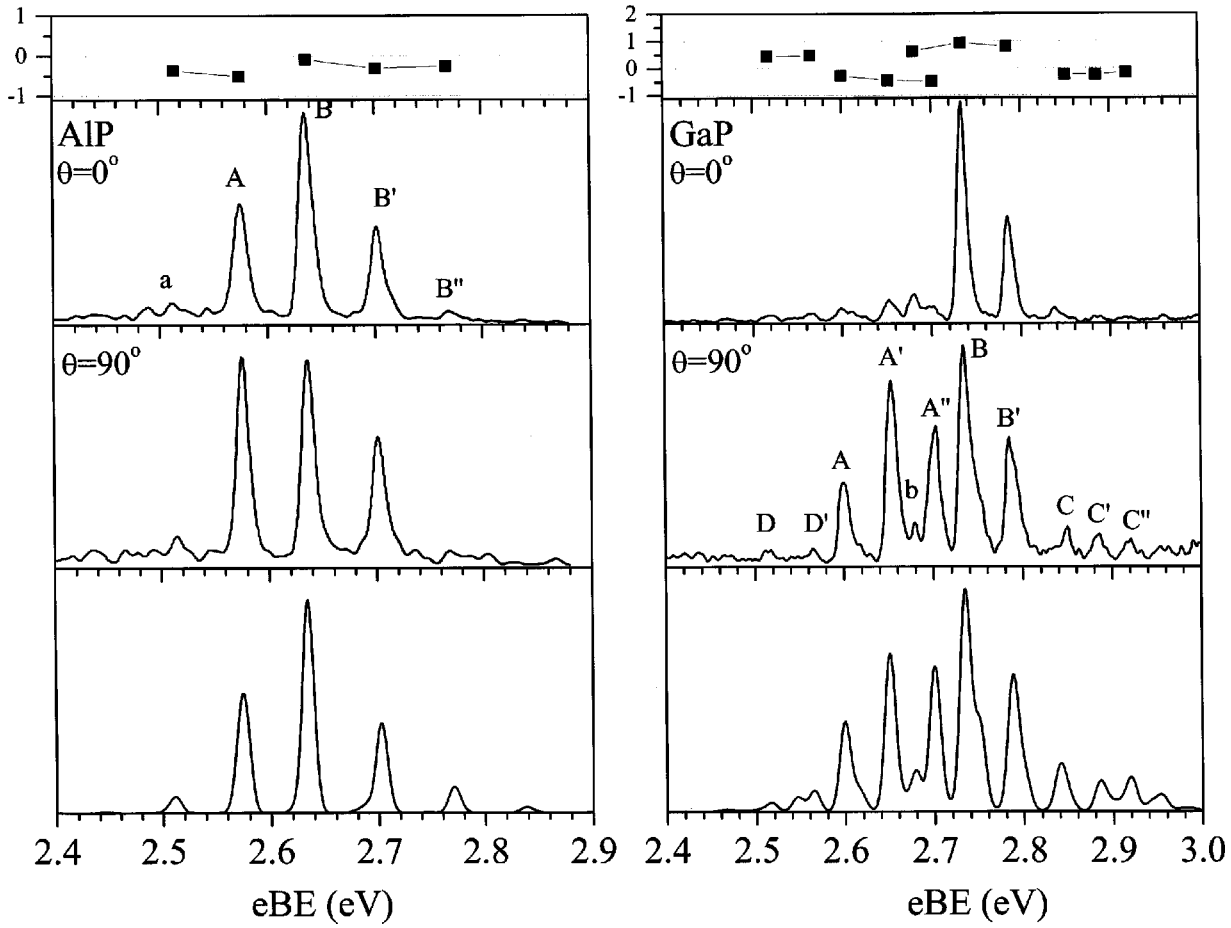

FIG. 5. Anion photoelectron spectra of AlP^- and GaP^- singlet manifold taken at 498 nm and laser polarization angles of $\theta=90°$ and $\theta=0°$. Experimental β parameters at the same photon energy are plotted in the top panel. FC simulation of the $\theta=90°$ ($\theta=0°$ for AlP) spectrum is shown in the bottom panel.

2. GaP

The β parameters plotted in the top panel of Fig. 5 show that the peaks can be divided into four bands. The two most intense progressions consist of peaks *A*, *A*, and *A″* and *b*, *B*, and *B′*. The three *A* peaks are spaced by 400 cm^{-1}, peaks *B* and *B′* are spaced by 435 cm^{-1}, while *b* and *B* are spaced by 445 cm^{-1}. The spacings and intensities of the peaks indicate that *A* and *B* are the vibrational origins of two electronic bands, while *b* is a vibrational hot band.

The photoelectron angular distributions are similar to those for the AlP singlet manifold, in that the relative intensity of the *A* progression is higher at $\theta=90°$ than at $\theta=0°$ (even more so for GaP), suggesting the same assignment in which the *A* and *B* bands correspond to the $^1\Pi\leftarrow{}^2\Sigma^+$ and $^1\Sigma^+\leftarrow{}^2\Sigma^+$ photodetachment transitions, respectively. This assignment is consistent with electronic structure calculations, the results of which are summarized in Table II. Archibong[24] finds that GaP^- has a $^2\Sigma^+$ ground state with a vibrational frequency of 445 cm^{-1}, and a $^2\Pi$ excited state with a term value of 0.064 eV and a vibrational frequency of 371 cm^{-1}; the hot band frequency we observe, 445 cm^{-1}, is clearly in better agreement with the $^2\Sigma^+$ state. In addition, the experimental vibrational frequencies of 402 and 433 cm^{-1} for the $^1\Pi$ and $^1\Sigma^+$ states, respectively, implied by our assignment, are in good agreement with the calculated frequencies.[25] 387 and 439 cm^{-1}. The $^1\Sigma^+-{}^1\Pi$ resulting splitting of 0.133 eV is, however, somewhat larger than the calculated splitting, 0.049 eV.[25]

There are two additional weak bands in the GaP singlet manifold. Peaks *C*, *C′*, and *C″* are spaced by 285 cm^{-1}. The only electronic state calculated to have a similar frequency is the $^1\Delta$ state (278 cm^{-1}).[25] This state is also one-electron accessible from the $^2\Pi$ excited anion state and we assign peaks *C*, *C′*, and *C″* to the $^1\Delta\leftarrow{}^2\Pi$ transition. Peaks *D* and *D′* must then be due to the $^1\Pi\leftarrow{}^2\Pi$ transition, the only remaining one-electron transition that can contribute to the singlet manifold. The spacing between these peaks, 400 cm^{-1}, matches the vibrational frequency of the $^1\Pi$ state, but it is also close to the calculated frequency of the anion $^2\Pi$ state, 371 cm^{-1}. Thus, it is not obvious if peaks *D* and *D′* represent a vibrational progression in the neutral $^1\Pi$ state or the anion $^2\Pi$ state. This point is discussed further in the context of the GaP triplet manifold.

3. InP and GaAs

The InP and GaAs singlet manifolds in Fig. 6 each show two vibrational progressions with photoelectron angular distributions similar to those seen in the AlP and GaP singlet manifolds, so we assign bands "*A*" and "*B*" to the $^1\Pi\leftarrow{}^2\Sigma^+$ and $^1\Sigma^+\leftarrow{}^2\Sigma^+$ photodetachment transitions, respectively. In the InP^- spectrum, peaks *A* and *A′* are spaced by 319 cm^{-1}, while peaks *B*, *B′*, and *B″* are spaced by 350

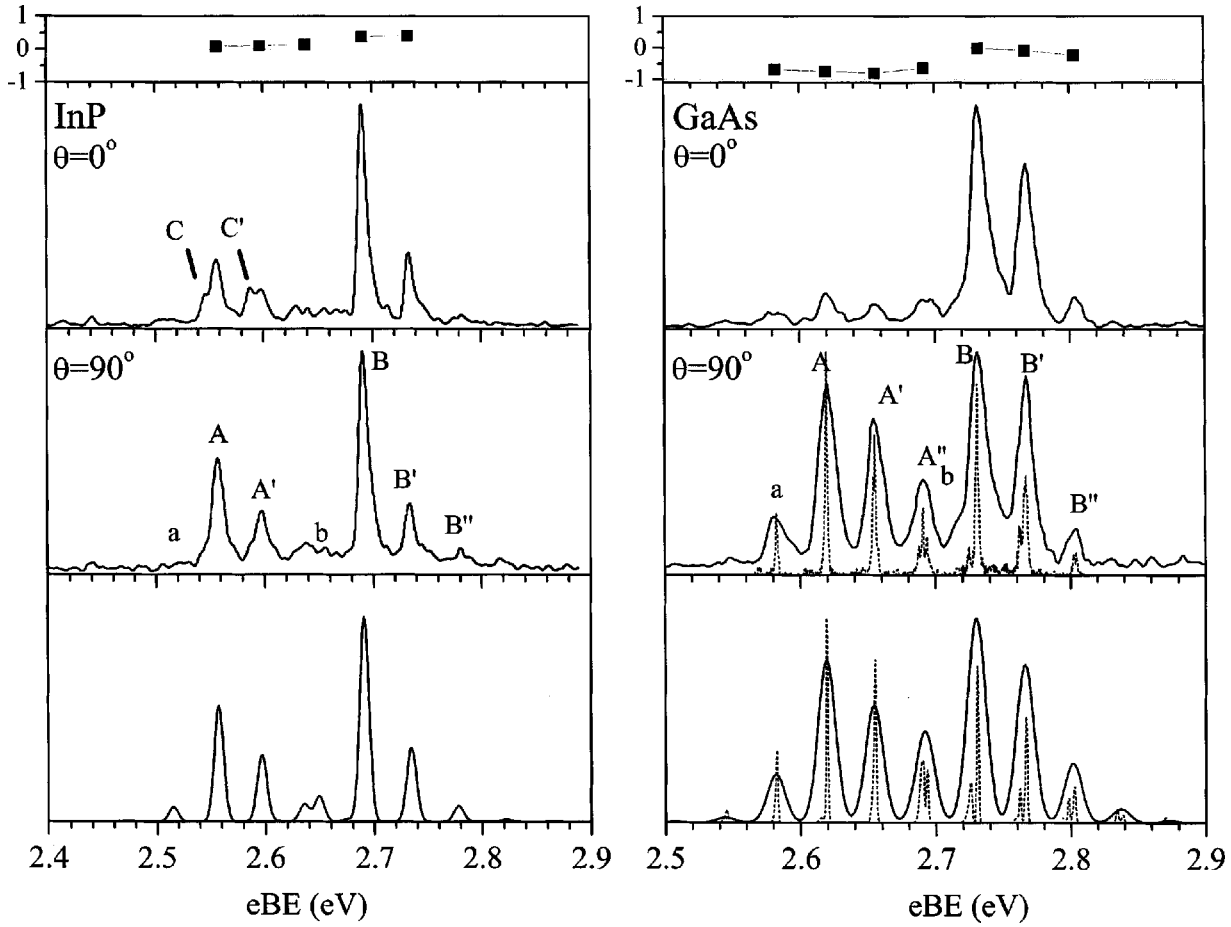

FIG. 6. Anion photoelectron spectra of InP^- and $GaAs^-$ singlet manifold taken at 355 nm (416 nm for InP) and laser polarization angles of $\theta=90°$ and $\theta=0°$. Experimental β parameters at the same photon energy are plotted in the top panel. FC simulation of the $\theta=90°$ spectrum is shown in the bottom panel. Experimental and simulated ZEKE spectra of $GaAs^-$ are shown as dotted lines in the lower two panels.

cm^{-1}; these correspond to the vibrational frequencies of the $^1\Pi$ and $^1\Sigma^+$ states, respectively, and the splitting between the two singlet states is 0.131 eV. These values can be compared to the calculation by Manna *et al.*[26] summarized in Table III. Note that Manna predicts the $^1\Delta$ state to lie between the $^1\Pi$ and $^1\Sigma^+$ states; we cannot verify this since no transitions to the $^1\Delta$ state are seen in our spectrum. Another feature of interest in the InP singlet manifold is that in the 0° spectrum, there are two partially resolved peaks (peaks *C* and *C′*, Fig. 6), each lying at 9 meV lower eBE than peaks *A* and *A′*. We believe these are $^1\Pi \leftarrow {}^2\Pi_{3/2}$ transitions, which would place the anion $^2\Pi_{3/2}$ state 9 meV above the $^2\Sigma^+$ ground state. This point is discussed further in our analysis of the InP triplet manifold.

TABLE I. Comparison of experimental and theoretical molecular constants of AlP.[a]

Method	$X\,^2\Sigma^+$	$A\,^2\Pi$	$X\,^3\Sigma^-$	$A\,^3\Pi_2$	$^3\Pi_1$	$^3\Pi$	$a\,^1\Pi$	$b\,^1\Sigma^+$	$c\,^1\Delta$	EA (eV)
GGA/DNP[b]	⋯	⋯	0.000	⋯	⋯	⋯	⋯	⋯	⋯	⋯
	⋯	⋯	348	⋯	⋯	⋯	⋯	⋯	⋯	⋯
	⋯	⋯	2.46	⋯	⋯	⋯	⋯	⋯	⋯	⋯
MRDCI[c]	0.00	0.08	⋯	⋯	⋯	⋯	⋯	⋯	⋯	1.90
	551	465	⋯	⋯	⋯	⋯	⋯	⋯	⋯	⋯
	2.163	2.273	⋯	⋯	⋯	⋯	⋯	⋯	⋯	⋯
MRDCI[d]	⋯	⋯	0.00	0.11	⋯	⋯	0.54	0.67	⋯	⋯
	⋯	⋯	359	449	⋯	⋯	487	528	⋯	⋯
	⋯	⋯	2.455	2.260	⋯	⋯	2.228	2.117	⋯	⋯
Experiment	0.000	0.082	0.000	0.108	0.117	0.128	0.516	0.574	⋯	2.043
	516	467	379	457	⋯	⋯	470	541	⋯	⋯
	2.163[c]	2.273[c]	2.40	2.26	⋯	⋯	2.22	2.10	⋯	⋯

[a]For each entry, the first row gives the term energy (in eV), the second row gives the vibrational frequency (in cm^{-1}), and the third row gives the bond length (in Å). Experimental term energies and frequencies have uncertainties of ±0.010 eV and ±15 cm^{-1}, respectively.
[b]From Ref. 51.
[c]From Ref. 22.
[d]From Ref. 23.

TABLE II. Comparison of experimental and theoretical molecular constants of GaP.[a]

Method	$X\ ^2\Sigma^+$	$A\ ^2\Pi_{3/2}$	$A\ ^2\Pi_{1/2}$	$X\ ^3\Sigma^-$	$A\ ^3\Pi_2$	$^3\Pi_1$	$^3\Pi$	$a\ ^1\Pi$	$b\ ^1\Sigma^+$	$c\ ^1\Delta$	EA (eV)
GGA/DNP[b]	⋯	⋯	⋯	0.000	⋯	⋯	⋯	⋯	⋯	⋯	⋯
	⋯	⋯	⋯	251	⋯	⋯	⋯	⋯	⋯	⋯	⋯
	⋯	⋯	⋯	2.76	⋯	⋯	⋯	⋯	⋯	⋯	⋯
MRDCI[c]	⋯	⋯	⋯	0.00	0.089	0.098	0.103	0.695	0.744	1.094	⋯
	⋯	⋯	⋯	266	358	357	359	387	439	278	⋯
	⋯	⋯	⋯	2.498	2.260	2.258	2.257	2.229	2.105	2.478	⋯
CCSD(T)[d]	0.000	0.064	⋯	0.000	0.116	⋯	⋯	⋯	0.739	⋯	1.86
	447	371[e]	⋯	297	357[c]	⋯	⋯	⋯	445[c]	⋯	⋯
	2.163	2.291	⋯	2.473	2.263	⋯	⋯	⋯	2.126	⋯	⋯
Experiment	0.000	0.048	0.062	0.000	0.099	0.116	0.134	0.612	0.746	0.946	1.988
	445	386	⋯	283.6[f]	415	⋯	⋯	402	433	285	⋯
	2.163[d]	2.291[d]	⋯	2.45	2.24	⋯	⋯	2.25	2.11	2.35	⋯

[a]For each entry, the first row gives the term energy (in eV), the second row gives the vibrational frequency (in cm^{-1}), and the third row gives the bond length (in Å). Experimental term energies and frequencies from this work have uncertainties of ±0.010 eV and ±15 cm^{-1}, respectively.
[b]From Ref. 51.
[c]From Ref. 25.
[d]From Ref. 24.
[e]B3LYP Frequency (cm^{-1}).
[f]Experimental value from Ref. 16.

The ZEKE spectrum of $GaAs^-$ shows that peaks *A*, *A′*, and *A″* form a progression with a frequency of 287.0 ±0.5 cm^{-1} and peak *a* is a hot band transition, giving an anion frequency of 298.0±0.5 cm^{-1}. Peaks *B*, *B′*, and *B″* form another progression with a frequency of 292.5 ±0.5 cm^{-1}, where peak *b* is a hot band transition with the same anion frequency of 298.0 cm^{-1}. The two bands thus originate from the same anion state, as expected. Based on our assignment, the vibrational frequency of the anion $^2\Sigma^+$ state is 298.0 cm^{-1}, and the neutral $^1\Pi$ and $^1\Sigma^+$ are states split by 0.114±0.001 eV. We see no significant contributions of transitions from excited anion electronic states.

Our results can be compared to theory with reference to Table IV. Balasubramanian's[42] calculation of 303 cm^{-1} for the $^2\Sigma^+$ ground state frequency is in closer agreement with our measurement than Meier's value[17] of 248 cm^{-1} multireference double configuration interaction (MRDCI). Manna and Das[20] have the closest calculated $^1\Pi-{}^1\Sigma^+$ energy separation, 0.082 eV. All other calculations overestimate this splitting by a factor of 2.[17–19]

C. Triplet manifolds

As noted in Sec. III, the photoelectron angular distributions for all the triplet manifolds indicated that each was composed of three distinct electronic photodetachment transitions. Figure 1 shows that there are three one-electron transitions from the anion $^2\Sigma^+$ and $^2\Pi$ states to the neutral triplet states: the $^3\Pi\leftarrow{}^2\Sigma^+$, $^3\Pi\leftarrow{}^2\Pi$, and $^3\Sigma^-\leftarrow{}^2\Pi$ transitions. Our analysis of the singlet manifolds indicates that all four diatomics have $^2\Sigma^+$ anion ground states, so if the energy ordering in Fig. 1 is correct, then the $^3\Pi\leftarrow{}^2\Sigma^+$ band will occur at the highest eBE, and the $^3\Sigma^-\leftarrow{}^2\Pi$ at the lowest. These considerations are a reasonable starting point for our analysis of the triplet manifolds. The anion vibra-

TABLE III. Comparison of experimental and theoretical molecular constants of InP.[a]

Method	$X\ ^2\Sigma^+$	$A\ ^2\Pi_{3/2}$	$A\ ^2\Pi_{1/2}$	$X\ ^3\Sigma_1^-$	$X\ ^3\Sigma_{0+}^-$	$A\ ^3\Pi_2$	$^3\Pi_1$	$^3\Pi_{0+}$	$^3\Pi_{0-}$	$a\ ^1\Pi$	$c\ ^1\Sigma^+$	$b\ ^1\Delta$	EA (eV)
MRDCI[b]	⋯	⋯	⋯	0	0.005	0.262	0.296	0.319	0.323	0.921	1.153	1.053	⋯
	⋯	⋯	⋯	251	249	290	289	290	289	327	305	261	⋯
	⋯	⋯	⋯	2.70	2.70	2.51	2.50	2.51	2.51	2.46	2.38	2.68	⋯
B3LYP[c]	0.00	⋯	⋯	0.00	⋯	⋯	⋯	⋯	⋯	1.057	⋯	⋯	1.594
	338	⋯	⋯	265	⋯	⋯	⋯	⋯	⋯	343	⋯	⋯	⋯
	2.382	⋯	⋯	2.526	⋯	⋯	⋯	⋯	⋯	2.326	⋯	⋯	⋯
QCISD(T)[c]	0.00	⋯	⋯	0.00	⋯	⋯	⋯	⋯	⋯	0.691	⋯	⋯	1.105
	340	⋯	⋯	255	⋯	⋯	⋯	⋯	⋯	329	⋯	⋯	⋯
	2.420	⋯	⋯	2.558	⋯	⋯	⋯	⋯	⋯	2.361	⋯	⋯	⋯
Experiment	0.000	0.009	0.087	0.000	⋯	0.151	0.187	0.210	0.224	0.669	0.800	⋯	1.845
	335	245	⋯	255	⋯	285	⋯	⋯	⋯	319	350	⋯	⋯
	2.43	2.51	⋯	2.70[b]	⋯	2.51[b]	⋯	⋯	⋯	2.49	2.39	⋯	⋯

[a]For each entry, the first row gives the term energy (in eV), the second row gives the vibrational frequency (in cm^{-1}), and the third row gives the bond length (in Å). Experimental term energies and frequencies have uncertainties of ±0.010 eV and ±15 cm^{-1}, respectively.
[b]From Ref. 26.
[c]GAUSSIAN 98 calculation using Los Alamos effective core potential basis set (LANL2DZ).

TABLE IV. Comparison of experimental and theoretical molecular constants of GaAs.[a]

Method	$X\ ^2\Sigma^+$	$A\ ^2\Pi_{3/2}$	$^2\Pi_{1/2}$	$X\ ^3\Sigma_1^-$	$X\ ^3\Sigma_{0+}^-$	$A\ ^3\Pi_2$	$^3\Pi_1$	$^3\Pi_{0+}$	$^3\Pi_{0-}$	$a\ ^1\Pi$	$b\ ^1\Sigma^+$	$c\ ^1\Delta$	EA (eV)
MRDCI[b]	0.00	0.02	⋯	0.00	⋯	0.17	⋯	⋯	⋯	0.74	0.90	0.94	1.51
	248	212	⋯	202	⋯	260	⋯	⋯	⋯	278	277	210	⋯
	2.333	2.471	⋯	2.598	⋯	2.381	⋯	⋯	⋯	2.350	2.249	2.593	⋯
CASSCF[c]	0.00	0.099	⋯	0.00	⋯	0.227	⋯	⋯	⋯	0.798	0.963	0.976	1.4
	303	216	⋯	215	⋯	236	⋯	⋯	⋯	277	279	214	⋯
	2.268	2.426	⋯	2.60	⋯	2.38	⋯	⋯	⋯	2.34	2.23	2.58	⋯
MRDCI[d]	⋯	⋯	⋯	0.00	0.009	0.091	0.151	0.217	0.221	0.7789	0.861	1.087	⋯
	⋯	⋯	⋯	180	181	234	240	234	231	265	297	189	⋯
	⋯	⋯	⋯	2.673	2.667	2.396	2.388	2.389	2.401	2.356	2.218	2.649	⋯
LDF[e]	⋯	⋯	⋯	0.00	⋯	⋯	⋯	⋯	⋯	⋯	⋯	⋯	1.89
	⋯	⋯	⋯	209	⋯	⋯	⋯	⋯	⋯	⋯	⋯	⋯	⋯
	⋯	⋯	⋯	2.65	⋯	⋯	⋯	⋯	⋯	⋯	⋯	⋯	⋯
Experiment	0.000	0.052	0.119	0.000	0.0053[f]	0.100	0.133	0.157	0.176	0.717	0.831	⋯	1.949
	298±0.5	242	⋯	213.12[f]	208.90[f]	263	⋯	⋯	⋯	287±0.5	292.5±0.5	⋯	⋯
	2.268[c]	2.426[c]	⋯	2.517[f]	2.548[f]	2.318	⋯	⋯	⋯	2.328	2.218	⋯	⋯

[a]For each entry, the first row gives the term energy (in eV), the second row gives the vibrational frequency (in cm^{-1}), and the third row gives the bond length (in Å). Experimental term energies and frequencies from this work have uncertainties of ±0.010 eV and ±15 cm^{-1}, respectively, except as noted.
[b]From Refs. 17 and 18.
[c]From Ref. 19.
[d]From Ref. 20.
[e]From Ref. 21.
[f]Experimental values from Ref. 13.

tional frequencies determined through observation of hot bands in the singlet manifolds are also useful in analyzing the triplet manifolds.

1. AlP

The triplet manifolds of the AlP^- PE spectra taken at 498 nm and polarization angles of $\theta=90°$ and $\theta=0°$ are shown in Fig. 3. From the β parameters in the top panel we identify three distinct bands: "*A*," "*B*," and "*C*." In band "*A*," peaks *A* and *A′* are separated by ~460 cm^{-1}. The peaks that make up band "*B*," peaks *b*, *B*, *B′*, and *B″*, all appear as partially resolved triplets with an average separation of 9–10 meV. The spacing between peaks *b* and *B* is around 515 cm^{-1}, while the spacing between peaks *B*, *B′*, and *B″* is around 460 cm^{-1}. Peaks *c*, *C*, and *C′* are very weak; the spacing between *c* and *C* is ~470 cm^{-1}, while peaks *C* and *C′* are separated by ~380 cm^{-1}.

The general considerations outlined above suggest that band "*B*" be assigned to the $^3\Pi \leftarrow ^2\Sigma^+$ transition, band "*A*" to the $^3\Pi \leftarrow ^2\Pi$ transition, and band "*C*" to the $^3\Sigma^- \leftarrow ^2\Pi$ transition. Although no clear evidence for transitions from the $^2\Pi$ state in AlP^- was seen in the singlet manifold, this state is predicted to lie only 0.08 eV above the $^2\Sigma^+$ ground state,[22] so some population of this state in the laser ablation source is expected. According to this assignment, band "*A*" results from detachment from a σ molecular orbital, whereas bands "*B*" and "*C*" result from detachment from the same π orbital. The observation that the anisotropy parameters of bands "*B*" and "*C*" are similar but very different from that for band "*A*" is qualitatively consistent with our assignment of the three bands. We note the triplet manifolds of the PE spectra of Si_2^- and Ge_2^- showed three photodetachment detachment transitions with similar polarization dependencies as bands "*A*"–"*C*" and analogous assignments were made.[28–30]

There are several more stringent tests of this assignment. Taking peak *b* as a hot band yields an anion vibrational frequency of ~515 cm^{-1}, essentially identical to the anion $^2\Sigma^+$ frequency determined from the AlP singlet manifold. Assuming peak *c* is a vibrational hot band, then band "*C*" originates from an anionic electronic state with frequency 460–470 cm^{-1}, in good agreement with the calculated anion frequency of 465 cm^{-1} for the anion $^2\Pi$ state.[22] The anion frequencies thus support the proposed assignment for two of the three bands.

The partially resolved triplet structure of band "*B*" is consistent with a $^3\Pi \leftarrow ^2\Sigma^+$ transition, with the triplets corresponding to transitions to the $\Omega=2$, 1, and 0 fine structure components of the neutral $^3\Pi$ state. Although no calculations of this fine structure have been reported, the 9–10 meV splitting we observe is comparable to the 7–8 meV splitting in the analogous $^3\Pi_u$ state of Si_2.[28] The spacing between peaks *B*, *B′*, and *B″* of 460 cm^{-1} is close to the calculated vibrational frequency of 449 cm^{-1} for the AlP $^3\Pi$ state.[23]

In band "*A*," the spacing between peaks *A* and *A′* is also 460 cm^{-1}, consistent with its assignment as a transition to the $^3\Pi$ state in AlP. However, if these peaks are from the $^3\Pi \leftarrow ^2\Pi$ transition, one can have as many as six fine structure contributions to each peak, namely transitions to the $^3\Pi_2$, $^3\Pi_1$, and $^3\Pi_0$ states from each of the (presumably) closely spaced anion $^2\Pi_{3/2}$ and $^2\Pi_{1/2}$ fine structure states. If all six transitions were active, one might not expect to resolve them because of differing fine structure splittings in the anion and neutral, but one would expect the peaks *A* and *A′* to be at least as broad as the peaks in band "*B*." This, however, is not the case. A possible explanation is that the neutral fine structure states are not accessed with equal intensity when the σ electron of the anion $^2\Pi$ state is detached. In fact, the photoelectron spectra of Ge_2^- and Sn_2^- show a strong $\Delta\Omega=\pm 1/2$ propensity rule for $^3\Pi \leftarrow ^2\Pi$

transitions.[27,29,31] If this rule holds for AlP^-, then photodetachment from the anion $^2\Pi_{3/2}$ state would yield the neutral $^3\Pi_2$ and $^3\Pi_1$ states, while the $^2\Pi_{1/2}$ state would yield the $^3\Pi_1$ and $^3\Pi_0$ states. As long as the anion and neutral fine structure splitting are similar, one would expect four overlapped transitions covering a narrower energy range that the triplets in band "*B*," consistent with our observations.

Peaks *c*, *C*, and *C'* are assigned to the $^3\Sigma^- \leftarrow ^2\Pi$ band. As mentioned above, the $c-C$ spacing is consistent with this assignment, as is the $C-C'$ spacing of 379 cm^{-1}, which is close to the calculated frequency of 359 cm^{-1} for the neutral $^3\Sigma^-$ state.[23] Figures 3 and 5 show the simulation of both the triplet and singlet manifolds of the AlP^- photoelectron spectrum. The parameters used in this simulation are listed in Table I, where they can be readily compared to previously determined theoretical values. Since the PE spectra are sensitive only to changes in the bond length upon photodetachment, the calculated anion bond lengths for the two anion states were assumed to be correct, and the neutral bond lengths were varied to reproduce the experimental spectrum.

In the singlet manifold, the vibrational frequency of the $^1\Pi$ state is taken to be the same as the spacing between peaks *A* and *B* in Fig. 5, so that peak *B* has a contribution from the transition to the $^1\Pi$ ($v=1$) level. In the triplet manifold, only a small change in bond length upon photodetachment is needed to reproduce the short vibrational progression associated with band "*A*," whereas more substantial changes are needed to reproduce the longer progressions associated with bands "*B*" and "*C*." These trends are consistent with the calculated bond lengths, further supporting our assignment of the photodetachment transitions. In addition, we find good agreement between experimental and theoretical term values for both the anion and neutral states. Finally, although we do not directly observe the $^3\Sigma^- - ^2\Sigma^+$ photodetachment transition, the adiabatic electron affinity of AlP, which corresponds to the energy difference between the $v=0$ levels of these two states, can be extracted our data using the assignments in Table I via

$$\mathrm{EA} = \mathrm{eBE}(C) + (\mathrm{eBE}(B) - \mathrm{eBE}(A)), \tag{4}$$

where *A*, *B*, and *C* are the vibrational origins of the three bands, with *B* taken to be the energy of the transition to the $^3\Pi_2$ fine structure component. Equation (4) yields EA(AlP) $= 2.043 \pm 0.020$ eV, close to the theoretical value[22] of 1.90 eV.

2. GaP

The triplet manifolds of the GaP^- PE spectra at $\theta = 0°$ and 90° in Fig. 3 share many similarities with the AlP^- triplet manifolds and a similar assignment should apply. However, the spin–orbit splittings in the $^3\Pi$ and $^2\Pi$ states of GaP and GaP^- should be larger than in the corresponding AlP states. With this in mind, peaks $B_{1,2,3}$ and $B'_{1,2}$ are assigned to the $^3\Pi - ^2\Sigma^+$ transition, peaks *a*, *A*, and *A'* to the $^3\Pi \leftarrow ^2\Pi$ transition, and peaks $c'-C'$ to the $^3\Sigma^- \leftarrow ^2\Pi$ transition. We now examine each of these assignments in more detail.

The five peaks $B_1 - B'_2$ are approximately equally spaced by 16–18 meV, or 130–145 cm^{-1}. This splitting is considerably less than the calculated vibrational frequencies for any GaP^- or GaP states (see Table II), and is more reasonably assigned to the spin–orbit splitting in the neutral $^3\Pi$ state. We therefore expect each $^3\Pi(\nu') - ^2\Sigma^+(\nu'')$ transition to yield a triplet of peaks with this characteristic spacing. The observed spin–orbit splitting of ~17 meV is about twice the value calculated by Manna.[25] The most straightforward assignment of these peaks is to take B_1 as the $^3\Pi_2(\nu' = 0) - ^2\Sigma^+(\nu'' = 0)$ transition, B_2 and B_3 as the transitions to the $^3\Pi_1$ and $^3\Pi_0(\nu' = 0)$ levels, respectively, and B'_1 and B'_2 as the $^3\Pi_2(\nu' = 1) - ^2\Sigma^+(\nu'' = 0)$ and $^3\Pi_1(\nu' = 1) - ^2\Sigma^+(\nu'' = 0)$ transitions, respectively. This assignment yields a vibrational frequency of 415 cm^{-1} for the $^3\Pi$ state, which disagrees with the calculated vibrational frequency[24,25] of 358 cm^{-1}.

Peaks *c*, *C*, and *C'* at low eBE consist of partially resolved doublets split by 12–14 meV. The doublet splitting could represent the spin–orbit splitting in the $^2\Pi$ state into its $^2\Pi_{3/2}$ and $^2\Pi_{3/2}$ components, and this doublet structure is consistent with assignment of these peaks to the $^3\Sigma^- \leftarrow ^2\Pi$ band. Peaks *c'*, *c*, and *C* are separated by approximately 370 cm^{-1}. This spacing agrees with the calculated frequency for the $^2\Pi$ anion state, suggesting these three peaks are ($\nu' = 0 \leftarrow \nu'' = n$) hot band transitions originating from the $^2\Pi_{3/2,1/2}$ states. The simulations presented below, using the $^3\Sigma^-$ experimental frequency determined by Li *et al.* of 286 cm^{-1},[16] suggest that peak *C* is the vibrational origin of the $^3\Sigma^- \leftarrow ^2\Pi$ band.

Peaks *a* and *A* are separated by 386 cm^{-1}, while peaks *A* and *A'* are separated by ~405 cm^{-1}. The relative intensities of these peaks suggest that peak *A* is the origin of the electronic transition, and *a* is a hot band of the same electronic transition. The $a-A$ splitting is close to the calculated vibrational frequency of the anion $^2\Pi$ state, 371 cm^{-1}, and the $A-A'$ splitting is similar to the frequency obtained from the series of peaks "*B*" (415 cm^{-1}). These observations support our assignment of peaks *a*, *A*, and *A'* to the $^3\Pi \leftarrow ^2\Pi$ transition. The finer structure of peak *A* (A_0 and A_1 center panel) depends on the individual spin–orbit splittings of the $^2\Pi$ and $^3\Pi$ states. From the "*B*" series of peaks we have determined the splitting in the $^3\Pi$ state to be 17–18 meV, and from the "*C*" series of peaks it appears the splitting in the $^2\Pi$ state is 14 meV. If we assumed GaP will exhibit the same behavior of Ge_2^- and Sn_2^- showing a strong $\Delta\Omega = \pm 1/2$ propensity, we should expect four transitions in a range of energy of about 21 meV. Simulation of these four states convoluted with our experimental resolution results in two peaks separated by approximately 17–18 meV, close to the $A_0 - A_1$ of ~15 meV.

Simulations of the GaP singlet and triplet manifold are shown in Figs. 3 and 5 and the parameters used in these simulations are given in Table II. The best simultaneous fit of the two manifolds leads to an assignment of peak *D'* in the singlet spectrum to the origin of the $^1\Pi \leftarrow ^2\Pi$ band. The triplet spectrum is the hardest to fit of all those reported in this paper; the contribution from hot bands is larger, and the peak spacing due to vibrational progressions and spin–orbit interactions are comparable. The discrepancy between the experimental and calculated $^3\Pi$ vibrational frequencies, 415

versus 358 cm^{-1}, is somewhat troubling, but the experimental value is needed to fit bands "*A*" and "*B.*" In any case, this is the best fitting of the singlet and triplet manifolds that we have been able to construct. We can determine the electron affinity of GaP in a manner similar to AlP, finding a value of 1.988 ± 0.020 eV.

3. InP

Anion photoelectron spectra of the triplet manifold of InP taken at 416 nm and a polarization angle of $\theta = 0°$ (top) and $\theta = 90°$ are shown in Fig. 4. The $\theta = 0°$ spectrum is dominated by peak A_1; the intensity of this peak drops off considerably at 90°, where it is one component of a partially resolved doublet with the other component labeled B_1. Peaks $B_1 - B_4$ and several peaks at higher eBE are the most prominent features at 90°. In addition there is a progression $c - C''$ at 90° that is absent at 0°.

Following our analysis of AlP and GaP, we assign peaks A_0, *a*, A_1, and A' to the $^3\Pi - ^2\Pi$ transition, peaks $B_1 - B_4$ and higher to the $^3\Pi - ^2\Sigma^+$ transition, and $c - C''$ to the $^3\Sigma^- - ^2\Pi$ transition. However, several features of interest appear in the InP triplet manifold that were not seen for the lighter molecules. The spacings between peaks $B_1 - B_4$ are 34, 23, and 14 meV. This uneven spacing is in contrast to the equally spaced triplets in AlP and GaP that were assigned to the $^2\Pi_{2,1,0}$ spin–orbit multiplet. The InP pattern reflects that expected for Hund's case (*c*) coupling, in which the splitting of the $^3\Pi_0$ component to $^3\Pi_{0+}$ and $^3\Pi_{0-}$ states becomes significant, suggesting that peaks $B_1 - B_4$ be assigned to transitions to the $^3\Pi_2$, $^3\Pi_1$, $^3\Pi_{0+}$, and $^3\Pi_{0-}$ states. Manna *et al.*[26] have calculated the splittings between these states to be 34, 23, and 4 meV, in partial agreement with our values.

Peaks A_1 and B_1 form a doublet separated by 9 meV in the $\theta = 90°$ spectrum. This is the same splitting in several doublets of the InP singlet manifold (Fig. 6). Our assignment of these doublets to transitions originating from the nearly degenerate anion $^2\Pi_{3/2}$ and $^2\Sigma^+$ states is consistent with assigning peak A_1 to the $^3\Pi_2(\nu = 0) \leftarrow ^2\Pi_{3/2}(\nu = 0)$ transition. Peak A' appears to comprise more than one transition; likely candidates are the $^3\Pi_1(\nu = 0) \leftarrow ^2\Pi_{3/2}(\nu = 0)$ and $^3\Pi_2(\nu = 1) \leftarrow ^2\Pi_{3/2}(\nu = 0)$ transitions. Based on our spin-orbit splittings determined above, and the calculated frequency of 290 cm^{-1} for the $^3\Pi$ state,[26] these transitions should occur at 34 and 36 meV, respectively, higher eBE than peak A_1. Peak *a* may be a vibrational hot band of peak *A*, yielding a vibrational frequency of 245 cm^{-1} for the $^2\Pi_{3/2}$ state. Finally, peak A_0, which lies at 0.042 eV lower eBE than peak A_1, could originate from the anion $^2\Pi_{1/2}$ state, and would correspond to the $^3\Pi_1 \leftarrow ^2\Pi_{1/2}$ vibrational origin if the anion $^2\Pi_{1/2} - ^2\Pi_{3/2}$ splitting were 78 meV.

The spacing of peaks *c* and *C* is around ~ 330 cm^{-1}, while that for peaks *C*, *C'*, and *C''* is around ~ 260 cm^{-1}, matching the experimental neutral ground state frequency of 258 cm^{-1}.[15] We thus assign peak *C* to the origin of the $^3\Sigma \leftarrow ^2\Pi_{3/2}$ transition. Using our assignment we can determine the electron affinity of InP in a similar manner to GaP and AlP, finding a value of 1.845 ± 0.020 eV.

In the absence of any prior experimental or theoretical information on InP^-, we performed electronic calculations on the anion and few states on the neutral. Geometries and frequencies were obtained using B3LYP (Becke-3-parameter-Lee–Yang–Parr)[45,46] exchange correlation functional and quadratic configuration interaction with double and triple excitation (QCISD(T)), using the LANL2DZ (Los Alamos ECP)[47] basis set in both calculations. Calculations were performed using GAUSSIAN 98[48] electronic structure package, and the results are summarized in Table III. The calculated anion frequencies are very close to that determined from the weak hot band *c* in the PE spectrum.

Based on the above considerations, a full simulation of the singlet and triplet manifolds is shown in Figs. 4 and 6 using the parameters in Table III. The FC simulation was performed assuming Manna's calculated bond lengths for the neutral $X\,^3\Sigma_1^-$ and $A\,^3\Pi_2$ states are correct.[26] From those we determine the anion and singlet bond lengths given in Table III. The simulation reproduces nearly all the features in the experimental spectra in both manifolds and shows, for example, that the peaks to high eBE of peaks $B_1 - B_4$ are transitions to vibrationally excited levels of the neutral $^3\Pi$ state.

4. GaAs

The GaAs triplet manifold (Fig. 4) is generally similar to the InP triplet manifold and analogous assignments should hold. The ZEKE spectrum, which resembles the 90° spectrum much more than the 0° spectrum, supports our overall assignment scheme in the following sense. Peaks A_0, A_1, and A', which should correspond to $^3\Pi \leftarrow ^2\Pi$ transitions, disappear in both the ZEKE spectrum and the PE spectrum at 90°. In the isovalent homonuclear molecular Si_2, these transitions would involve detachment from a σ_g molecular orbital and are therefore not seen in the anion ZEKE spectrum because detachment from such an orbital cannot result in an $l = 0$ (*s*-wave) electron.[49,50] While this ZEKE transition is not strictly forbidden from heteronuclear $GaAs^-$, we might expect it to have a small *s*-wave partial cross section near threshold and hence be very weak.

Looking at the peak positions in more detail, $B_1 - B_4$ are spaced by 33, 24, and 19 meV, similar to the spacings for the analogous peaks in InP, and we assign these to the $^3\Pi_{2,1,0+,0-}(\nu' = 0) \leftarrow ^2\Sigma^+(\nu'' = 0)$ transitions. The peaks at higher eBE are assigned to transition to higher vibrational levels in the $^3\Pi$ state. Manna and Das[20] predicted the splitting in the $^3\Pi$ state to be 60, 66, 4, almost twice the determined values (except for the 0+/0− splitting). Our values are comparable with experimental splittings for the analogous $^3\Pi$ state in Ge_2.[29] The hot band b_1 yields a vibrational frequency of 298 cm^{-1} for the anion $^2\Sigma^+$ state, in agreement with our assignment of the singlet manifold.

Peaks A_0, A_1, and A' appear to have the same assignments as for InP. However, the $^2\Pi_{3/2} - ^2\Sigma^+$ splitting (between peaks A_1 and B_1) is 52 meV, noticeably larger than the value of 9 meV found for InP^-. The assignment of peak A_0 to the $^3\Pi_1 \leftarrow ^2\Pi_{1/2}$ transition implies a spin–orbit splitting of 0.067 eV in the anion $^2\Pi$ state, close to the InP^- splitting.

Peaks *c*, *C*, and *C'* are assigned to the $^3\Sigma^- - ^2\Pi$ transition similar to InP. The spacing between peaks *c* and *C* is

around 242 cm^{-1}, consistent with this band originating from a different anion electronic state than band "*B*." This frequency is slightly higher than that calculated by Balasubramanian[42] of 216 cm^{-1}. The spacing between peaks *C* and *C'* (~220 cm^{-1}) is consistent with the experimental neutral frequency of 213 cm^{-1} determined by Lemire *et al.*[13] We thus assign peak *C* as the origin of this band.

FC simulations of the singlet and triplet bands were generated using the parameters in Table IV. In this case, all bond length changes are referenced to the experimental bond length for the $^3\Sigma_1^-$ state, 2.517 Å, obtained from the rotationally resolved laser-induced fluorescence spectrum of GaAs.[13] The $^3\Sigma_{0+}^-$ state is not resolved but is included in Table IV for completeness. We find an electron affinity of 1.949 ± 0.020 eV using the same procedure as for the other diatomics. The $^2\Sigma - ^2\Pi$ splitting is in good agreement with the calculated splitting by Balasubramanian[19] of 0.099 eV. The electron affinities calculated by Balasubramanian and Meier *et al.* of 1.4 ± 0.02 eV second-order configuration interaction and 1.51 eV (MRDCI), respectively, are too low. However, Lou *et al.* report a much closer value of 1.89 eV employing the more empirical discrete Fourier transition method using the local density functional (LDF).[21]

V. DISCUSSION

The analysis in Sec. IV is fairly involved, and an evaluation of its strong and weak points is in order. In general, assignment of the singlet manifolds was straightforward and showed that all the anions have $^2\Sigma^+$ ground states. In the case of GaP and InP, the energy of the low-lying $^2\Pi$ state was obtained through the observation of electronic hot bands in the singlet manifold. The combination of photoelectron energy and angular distributions made it possible to distinguish clearly between different electronic photodetachment transitions, even if they were overlapped, and difference in peak spacings facilitated identification of the vibrational origin for each photodetachment transition.

The triplet manifolds are more problematic to assign. The identification and assignment of the $^3\Pi \leftarrow ^2\Sigma^+$ transitions (the "*B*" peaks) was generally straightforward because of their polarization dependence and multiplet pattern from spin–orbit splitting in the $^3\Pi$ state. Our reasoning in Sec. IV B makes us confident that the assignment of the "*A*" peaks to the $^3\Pi \leftarrow ^2\Pi$ transitions is correct, but this assignment does raise a few questions. In particular, at $\theta = 0°$, at least one peak associated with this transition dominates the PE spectrum, while in the singlet manifolds, electronic hot bands originating from the $^2\Pi$ state, are either small or indistinguishable from the noise, regardless of the laser polarization angle.

The high intensity of the "*A*" peaks is due to in part to a smaller change in geometry for the $^3\Pi \leftarrow ^2\Pi$ transition compared to the $^3\Pi \leftarrow ^2\Sigma^+$ transitions for all four species (see Tables I–IV), resulting in a much narrower Franck–Condon profile for the $^3\Pi \leftarrow ^2\Pi$ transition. In addition, photodetachment from the $^2\Sigma^+$ state accesses all the Ω levels of the $^3\Pi$ state with approximately equal intensity, whereas only one or two transitions to these Ω levels from the anion $^2\Pi$ state occur with appreciable intensity, further concentrating the $^3\Pi \leftarrow ^2\Pi$ transition in a smaller number of peaks. These effects may not be the whole story, however. The relative intensity of the "*A*" peaks is reduced in photoelectron spectra of the triplet manifolds of GaP^- and $GaAs^-$ at lower wavelengths, suggesting that non-Franck–Condon effects possibly due to the presence of an excited anion electronic state near 498 nm are distorting the intensity profile.

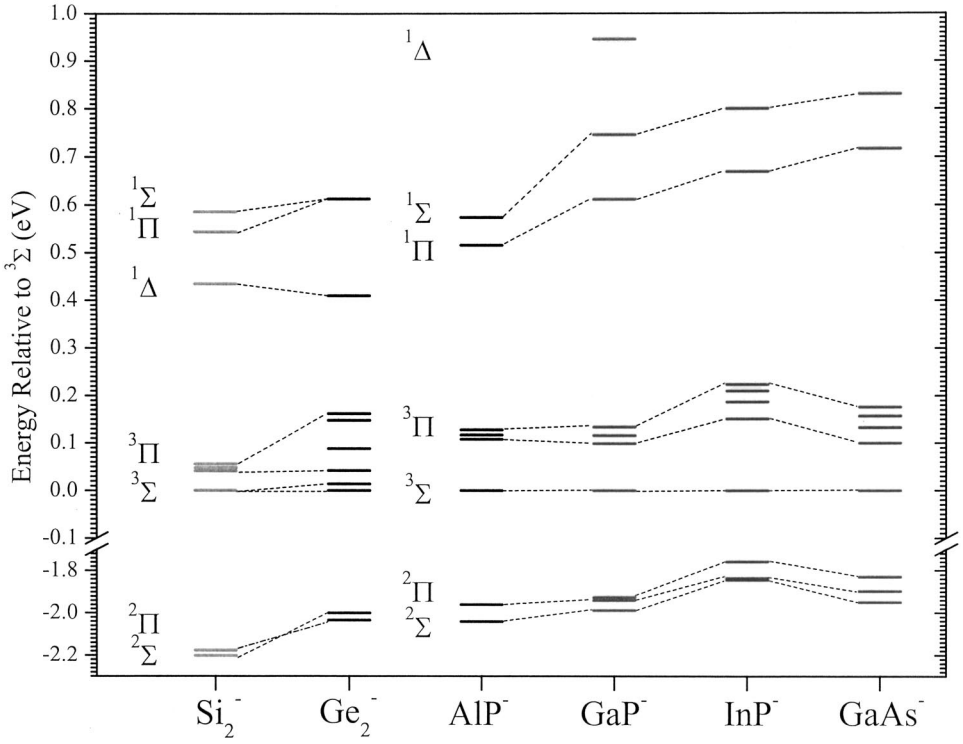

FIG. 7. Energy level diagram showing the electronic structure of the anion and neutral states of the isoelectronic species, Si_2, Ge_2, AlP, GaP, InP, and GaAs. The energy is referenced with respect to the $^3\Sigma$ state for each species.

The other issue regarding the $^3\Pi \leftarrow {}^2\Pi$ peaks is the intensity distribution among the Ω levels of the $^3\Pi$ state. We have invoked a $\Delta\Omega = \pm 1/2$ propensity rule based on other anion PE spectra to explain the reduced number of peaks, but even in InP and GaAs, where all the spin–orbit transitions are well separated, the intensities of the transitions that we assigned to the $\Omega' = 2 \leftarrow \Omega'' = 3/2$ and $\Omega' = 1 \leftarrow \Omega'' = 3/2$ are not the same. In the case of GaP the splittings in both states are comparable, resulting in a single partially resolved peak (A). A careful theoretical study of these open-shell photodetachment transitions would be of great use in understanding the observed intensities.

The "*C*" peaks assigned to the $^3\Sigma^+ \leftarrow {}^2\Pi$ are very important because they provide the only experimental means of determining the splitting between the neutral $^3\Pi$ and $^3\Sigma^-$ states as well as the electron affinity, since the $^3\Sigma^+ \leftarrow {}^2\Sigma^+$ transition which would provide a direct measure of the electron affinity is not one-electron allowed. The key issue with this transition is to be able to assign the vibrational origin, which can generally be done because the anion and neutral vibrational frequencies are different. We expect the error in the electron affinity to be higher than the other determined term energies for this reason.

Figure 7 shows a graphical comparison of the experimental ground and excited state energetics for the four III–V species studied here as well the homonuclear, isovalent species Si_2 and Ge_2. The figure shows that the electron affinity of the XP diatomics decreases as the mass of X increases from Al to In, while the electron affinities of GaP and GaAs are roughly equal. This trend suggests that the extra electron in the anion is localized more on the group III atom, a reasonable result in that the III–V neutrals are polar molecules with a partial negative charge on the more electronegative group V atom.

The main difference between the homonuclear and heteronuclear diatomics is in the singlet manifold. Electronic structure calculations predict the ordering of the excited singlet states is reversed in homonuclear versus heteronuclear species, and our experiments confirm this in all cases where transitions to the singlet states are seen; recall that GaP was the only III–V diatomic for which transitions to the $^1\Delta$ state were observed. Figure 7 also shows the consequences of the evolution from Hund's case (a)–(c) coupling, with spin–orbit splittings progressively increasing as the atoms become heavier, and measurable splittings of the $^3\Pi_0$ state into 0^+ and 0^- components for Ge_2, InP, and GaAs. The consequences of this evolution are also evident in the anions. In InP^-, the spin–orbit splitting in the $^2\Pi$ state results in the $\Omega = 3/2$ component lying only 9 meV above the $^2\Sigma^+$ state, while in Ge_2^- (and Sn_2^-) the $\Omega = 3/2$ level is pushed below the $^2\Sigma^+$ state.

ACKNOWLEDGMENT

This work is supported by the National Science Foundation under Grant No. DMR-0139064.

[1] A. P. Alivisatos, J. Phys. Chem. **100**, 13226 (1996).
[2] A. P. Alivisatos, Ber. Bunsenges. Phys. Chem. **101**, 1573 (1997).
[3] A. E. Douglas and G. Herzberg, Can. J. Res., Sect. A **18**, 179 (1940).
[4] O. A. Mosher and R. P. Frosch, J. Chem. Phys. **52**, 5781 (1970).
[5] H. Bredohl, I. Dubois, Y. Houbrechts, and P. Nzohabonayo, J. Phys. B **17**, 95 (1984).
[6] H. Bredohl, I. Dubois, Y. Houbrechts, and P. Nzohabonayo, J. Mol. Spectrosc. **112**, 430 (1985).
[7] C. J. Reid, Int. J. Mass Spectrom. Ion Processes **127**, 147 (1993).
[8] R. R. Reddy, A. S. R. Reddy, and T. V. R. Rao, Physica B & C **132B+C**, 373 (1985).
[9] M. Lorenz, J. Agreiter, A. M. Smith, and V. E. Bondybey, J. Chem. Phys. **104**, 3143 (1996).
[10] K. R. Asmis, T. R. Taylor, and D. M. Neumark, Chem. Phys. Lett. **295**, 75 (1998).
[11] H. Gomez, T. R. Taylor, and D. M. Neumark, J. Phys. Chem. A **105**, 6886 (2001).
[12] K. R. Asmis, T. R. Taylor, and D. M. Neumark, Chem. Phys. Lett. **308**, 347 (1999).
[13] G. W. Lemire, G. A. Bishea, S. A. Heidecke, and M. D. Morse, J. Chem. Phys. **92**, 121 (1990).
[14] M. Ebben and J. J. ter Meulen, Chem. Phys. Lett. **177**, 229 (1991).
[15] S. Li, R. J. Van Zee, and W. Weltner, Jr., J. Phys. Chem. **98**, 2275 (1994).
[16] S. Li, R. J. Van Zee, and W. Weltner, Jr., J. Phys. Chem. **97**, 11393 (1993).
[17] U. Meier, S. D. Peyerimhoff, and F. Grein, Chem. Phys. **150**, 331 (1991).
[18] U. Meier, S. D. Peyerimhoff, P. J. Bruna, and F. Grein, J. Mol. Spectrosc. **134**, 259 (1989).
[19] K. Balasubramanian, J. Phys. Chem. **94**, 7764 (1990).
[20] B. Manna and K. K. Das, J. Phys. Chem. A **102**, 9876 (1998).
[21] L. Lou, L. Wang, L. P. F. Chibante, R. T. Laaksonen, P. Nordlander, and R. E. Smalley, J. Chem. Phys. **94**, 8015 (1991).
[22] P. J. Bruna and F. Grein, J. Phys. B **22**, 1913 (1989).
[23] U. Meier, S. D. Peyerimhoff, P. J. Bruna, S. P. Karna, and F. Grein, Chem. Phys. **130**, 31 (1989).
[24] E. F. Archibong and A. St-Amant, Chem. Phys. Lett. **316**, 151 (2000).
[25] B. Manna and K. K. Das, J. Mol. Struct.: THEOCHEM **467**, 135 (1999).
[26] B. Manna, A. Dutta, and K. K. Das, J. Phys. Chem. A **104**, 2764 (2000).
[27] J. Ho, M. L. Polak, and W. C. Lineberger, J. Chem. Phys. **96**, 144 (1992).
[28] C. C. Arnold, T. N. Kitsopoulos, and D. M. Neumark, J. Chem. Phys. **99**, 766 (1993).
[29] C. C. Arnold, C. S. Xu, G. R. Burton, and D. M. Neumark, J. Chem. Phys. **102**, 6982 (1995).
[30] T. N. Kitsopoulos, C. J. Chick, Y. Zhao, and D. M. Neumark, J. Chem. Phys. **95**, 1441 (1991).
[31] V. D. Moravec, S. A. Klopcic, and C. C. Jarrold, J. Chem. Phys. **110**, 5079 (1999).
[32] R. B. Metz, A. Weaver, S. E. Bradforth, T. N. Kitsopoulos, and D. M. Neumark, J. Phys. Chem. **94**, 1377 (1990).
[33] C. Xu, G. R. Burton, T. R. Taylor, and D. M. Neumark, J. Chem. Phys. **107**, 3428 (1997).
[34] T. R. Taylor, H. Gomez, K. R. Asmis, and D. M. Neumark, J. Chem. Phys. **115**, 4620 (2001).
[35] B. A. Mamyrin and D. V. Shmikk, Sov. Phys. JETP **76**, 1500 (1979).
[36] G. Markovich, R. Giniger, M. Levin, and O. Cheshnovsky, J. Chem. Phys. **95**, 9416 (1991).
[37] J. Cooper and R. N. Zare, in *Lectures in Theoretical Physics*, edited by S. Geltman, K. T. Mahanthappa, and W. E. Brittin (Gordon and Breach, New York, 1969), Vol. XI-C, pp. 317–337.
[38] K. M. Ervin and W. C. Lineberger, in *Advances in Gas Phase Ion Chemistry* (JAI Press Inc., Greenwich, CT, 1992), Vol. 1, pp. 121–166.
[39] C. C. Arnold, Y. X. Zhao, T. N. Kitsopoulos, and D. M. Neumark, J. Chem. Phys. **97**, 6121 (1992).
[40] T. N. Kitsopoulos, I. M. Waller, J. G. Loeser, and D. M. Neumark, Chem. Phys. Lett. **159**, 300 (1989).
[41] K. Balasubramanian, J. Chem. Phys. **86**, 3410 (1987).
[42] K. Balasubramanian, J. Mol. Spectrosc. **139**, 405 (1990).
[43] K. Balasubramanian, J. Chem. Phys. **92**, 2123 (1990).
[44] U. Meier, S. D. Peyerimhoff, and F. Grein, Chem. Phys. **150**, 331 (1991).
[45] A. D. Becke, J. Chem. Phys. **98**, 1372 (1993).
[46] C. Lee, W. Yang, and R. G. Parr, Phys. Rev. B **37**, 785 (1988).
[47] C. F. Melius and W. A. Goddard III, Phys. Rev. A **10**, 1528 (1974).
[48] M. J. Frisch *et al.*, GAUSSIAN 98, Gaussian, Inc., Pittsburgh, PA, 1998.
[49] L. M. Branscomb, D. S. Burch, S. J. Smith, and S. Geltman, Phys. Rev. **111**, 504 (1958).
[50] E. P. Wigner, Phys. Rev. **73**, 1002 (1948).
[51] A. Costales, A. K. Kandalam, R. Franco, and R. Pandey, J. Phys. Chem. B **106**, 1940 (2002).